

## Beyond the orthogonal

### On the influence of build orientation on fatigue crack growth in SLM Ti-6Al-4V

Rans, Calvin; Michielssen, Jef; Walker, Megan; Wang, Wandong; Hoen-Velterop, Ludmila 't

**DOI**

[10.1016/j.ijfatigue.2018.06.038](https://doi.org/10.1016/j.ijfatigue.2018.06.038)

**Publication date**

2018

**Document Version**

Accepted author manuscript

**Published in**

International Journal of Fatigue

**Citation (APA)**

Rans, C., Michielssen, J., Walker, M., Wang, W., & Hoen-Velterop, L. . (2018). Beyond the orthogonal: On the influence of build orientation on fatigue crack growth in SLM Ti-6Al-4V. *International Journal of Fatigue*, 116, 344-354. <https://doi.org/10.1016/j.ijfatigue.2018.06.038>

**Important note**

To cite this publication, please use the final published version (if applicable). Please check the document version above.

**Copyright**

Other than for strictly personal use, it is not permitted to download, forward or distribute the text or part of it, without the consent of the author(s) and/or copyright holder(s), unless the work is under an open content license such as Creative Commons.

**Takedown policy**

Please contact us and provide details if you believe this document breaches copyrights. We will remove access to the work immediately and investigate your claim.

# Beyond the Orthogonal: On the Influence of Build Orientation on Fatigue Crack Growth in SLM Ti-6Al-4V

Calvin Rans\*, Jef Michielssen, Megan Walker, Wandong Wang

*Delft University of Technology, Kluyverweg 1, Delft, 2629 HS, the Netherlands*

Ludmila 't Hoen-Velterop

*NLR - Netherlands Aerospace Centre, Marknesse, 8316 PR, the Netherlands*

---

## Abstract

A challenge in developing an in-depth understanding of the crack growth resistance of Additively Manufactured materials is the fact that their mechanical properties have been shown to be both process and part-geometry dependent. Up to now, no studies have investigated the influence of off-axis (beyond the three orthogonal build orientations) orientations on the fatigue crack growth behaviour of selective laser melted Ti-6Al-4V. Furthermore, the widespread use of compact tension specimens for investigating the material behaviour generates data more suitable for plane-strain conditions, rather than the plane-stress state which is more applicable to many lightweight aerospace structures. To address this gap in knowledge, a comprehensive study was carried out to investigate the influence of off-axis build direction in thin SLM Ti-6Al-4V plates, with a focus on the influence of columnar grain orientation on the fatigue crack growth behaviour. It was found that although a macroscopic columnar grain structure is visible on the specimens, it had no discernible influence on the crack growth resistance when the specimen had undergone a stress relieving or HIP heat treatment.

### *Keywords:*

Additive Manufacturing, fatigue crack growth, Selective Laser Melting, anisotropy, Titanium

---

\*Corresponding Author

*Email address:* [C.D.Rans@tudelft.nl](mailto:C.D.Rans@tudelft.nl) (Calvin Rans)

## 1. Introduction

Additive Manufacturing (AM) is the “process of joining materials to make parts from 3D model data, usually layer upon layer” [1]. In contrast to formative (i.e. rolling, bending) and subtractive (e.g. machining, drilling, turning) processes the cost-effective minimum batch size is one [2, 3], parts can be produced at the point of use and on demand [2], material waste is minimized [2, 4] and complexity is free [2, 3, 4, 5].

One particular AM process known as powder bed fusion (PBF) constructs parts using fine powders as feedstock. In this process, powder is mechanically deposited onto a powder bed and an energy source is used to sinter or melt the powder together. Once a layer is complete, the powder bed moves down allowing a new layer of powder to be deposited; constructing a component with layers typically ranging from 0.03-0.1mm thick [6]. The part is constructed within an enclosed build chamber typically filled with an inert gas in order to minimize oxidation and degradation [6]. Selective Laser Melting (SLM) is one type of PBF process in which the heat source used to melt or fuse the particles together is a laser [1]. With the SLM process, lightweight metallic structures not possible to manufacture using traditional methods, can be produced. The use of these structures can result in significant improvement of the strength-to-weight ratio, making them of particular interest to the aerospace industry [4]. SLM may also bring about a reduction in fabrication costs within the aerospace sector due to elimination of highly wasteful conventional processes [4].

Titanium alloys, in particular Ti-6Al-4V have proven to be a popular choice for SLM [6]. Ti-6Al-4V is an  $\alpha+\beta$  alloy which in equilibrium at 800°C is composed of approximately 15vol.%  $\beta$  phase [7]. The alloy combines light weight with good strength, ductility, fatigue and fracture properties making it an ideal candidate for aerospace applications [7]. During the SLM process, high cooling rates (103-108K/sec) result in rapid solidification of the material [8]. The as-deposited microstructure of SLM Ti-6Al-4V is fully lamellar consisting of elongated columnar  $\beta$  grains (on the order of several hundred micrometres in length) and an acicular martensitic  $\alpha$  phase [9, 7, 10]. The higher cooling rates of the SLM process produce a finer lamellar structure than that which is typically seen in a casting [7]. In general, the  $\beta$  grains grow parallel to the build direction; however, their exact growth depends upon local heat transfer conditions which depend upon properties such as the scanning strategy and part geometry [10].

The directionality of the columnar grain structure in combination with the production of residual stresses and porosity can produce an anisotropic part. Leuders et al. [11] measured the residual stresses in as-built specimens, observing maximum residual stresses to vary between 265 MPa and 775 MPa in the two orthogonal directions within the build plane. These residual stresses were found to be effectively eliminated with an 800°C Stress Relieving heat treatment [11], a result that is confirmed by additional studies on stress relieving heat treatments within the literature [12]. The SLM process is also known to introduce porosity within a material that can influence strength and other material properties [13]. Optimization of the SLM process can help reduce porosity below a fraction of a percent [14], however, even small amounts of porosity can be detrimental to specific material properties such as fatigue crack initiation behaviour [11, 15, 16].

Post-processing heat treatments may be used to both homogenize the microstructure and to relieve residual stresses. These heat treatments are done at temperatures ranging from approximately 500-900°C for 1-4 hours followed by air or furnace cooling [9, 12]. Hot Isostatic Pressure (HIP) treatment may also be applied to reduce porosity. In this case the heat treatment is conducted under pressure.

For components to be used within the aerospace sector they must meet certification requirements. A common approach to certification with respect to fatigue and durability is the *Damage Tolerance* approach. In this approach, it is accepted that defects and damages may occur, and the structural integrity of a component is ensured by designing it such that any damage that does occur can be detected and repaired through regular inspections. This design philosophy is particularly relevant to AM produced parts due to the risk of manufacturing defects such as entrapped gas pores (porosity) and regions of incomplete fusion known as lack-of-fusion defects [16, 17, 18]. These defects act as stress risers that can accelerate the initiation of fatigue cracks within a component.

In order to apply the Damage Tolerance approach, a thorough understanding of the growth behaviour of potential damages (ie: cracks) is needed. Suitable inspection intervals for a component are based on the amount of time between when a crack is of sufficient size to be detected and when it will result in loss of structural integrity. Although we have an acceptable level of understanding of the crack growth behaviour of Ti-6Al-4V manufactured using traditional processes, this is not currently the case for SLM Ti-6Al-4V. As previously mentioned, one of the key characteristics of SLM Ti-6Al-4V is

the potential for anisotropic material properties due both to residual stresses and to the columnar grain structure aligned with the build direction.

There are six possible orientations for a component produced using AM as per ISO/ASTM 52921:2013(E): XYZ, XZY, YXZ, YZX, ZXY, ZYX [19]. These can be grouped into three categories as follows: XYZ/YXZ, XZY/YZX and ZXY/ZYX. Each one of groupings will have a different relationship between the direction of crack propagation and the build layer orientation. The crack propagates transverse, parallel or perpendicular to the build layers in the XYZ/YXZ, XZY/YZX and ZXY/ZYX orientations, respectively. In summary, literature published regarding the impact of anisotropy of SLM Ti-6Al-4V on the fatigue crack growth properties can be discussed in terms of three orientations hereafter referred to as either; transverse, perpendicular or parallel.

To date several studies have been conducted to investigate the presence of anisotropy in the fatigue crack growth properties of SLM Ti-6Al-4V. In general, these studies have reported that there is a great deal of experimental scatter in fatigue crack growth data for SLM Ti-6Al-4V in all three orthogonal orientations relative to conventionally manufactured Ti-6Al-4V [15, 11, 20, 21]. Some authors have reported that samples in the parallel orientations exhibit a greater extent of experimental scatter when compared to other orientations in the As-Built (AB) condition [11, 21]. Applying a Stress-Relief (SR) heat treatment, scatter decreases and fatigue crack growth behaviour is improved (relative to the AB condition) [11, 20]. Some authors have demonstrated that the fatigue crack growth behaviour following appropriate heat treatment (SR, HIP or HT) falls within the scatter band of traditionally manufactured Ti-6Al-4V [15, 11], indicating that the scatter in AB material may be caused by residual stresses.

Varying results have been published in the literature on the influence of build orientation. Dhansay et al. [15] and Edwards et al. [21] reported that there is no significant difference between the fatigue crack growth behaviour of SLM Ti-6Al-4V in the three orthogonal orientations in the AB condition, although Edwards observed a small influence on overall fracture toughness. However, Leuders et al. [11] reported that, in the fast crack growth regime, samples with crack growth occurring perpendicular to the layers had a favourable behaviour more closely matching that of SR or HIP counterparts. This crack growth behaviour fell within the scatter band of traditionally manufactured Ti-6Al-4V. Leuders [11] also reported that samples with crack growth occurring parallel to the build layers have a lower

fatigue crack growth threshold than other orientations in both the AB, SR and HIP state. Cain et al. [20] found that there is some effect of build orientation on fatigue crack growth properties which is most notable in the AB condition. In particular, it was noted that the perpendicular and parallel orientations exhibited higher crack growth rates than specimens in the transverse orientation.

A serious challenge in attempting to make sense of some of the above results in the literature is their link to processing parameters within the SLM process itself. It is clear that processing parameters such as scanning strategies, laser power and spot size should have an influence on the material state due to their direct importance on the melting and fusing process in SLM. However, even machine type, machine instance, part geometry, and many other variables can have an influence on the material state. Many studies in the literature, however, do not fully report all of these details. For instance, Dhansay et al. [15] report the machine type, layer thickness, and maximum power of the laser, while all other details of the fabrication process were not provided to the researchers by the specimen manufacturers. Similarly, Leuders [11] report the type of machine used, layer thickness, and powder diameter, but no other processing parameters. This is not a critique of the researchers themselves as it is recognized that many of these studies in the literature are done in collaboration with partners that want to keep aspects of their process proprietary. It could be further argued that a precise set of minimum necessary processing parameters is not established and that the precise link between all possible parameters and the resulting material state is not fully understood.

Several authors have reported that the fatigue crack growth behaviour is strongly dependent upon residual stresses [11, 20]. In both cases, the authors came to this conclusion via comparison of samples subjected to SR heat treatments and AB samples. In particular, Leuders et.al [11] was able to demonstrate by conducting heat treatments above and below  $\beta$ -transus that residual stresses, not microstructure, play the dominant role in dictating the fatigue crack growth properties of SLM Ti-6Al-4V. Furthermore, similar crack growth rates for both SR and HIP specimens demonstrate that porosity plays a minor role in the crack growth behaviour [11]. However, these studies have been limited to only the three orthogonal orientations with respect to the build platform.

A final observation on the experimental investigations of fatigue crack growth of SLM Ti-6Al-4V in the literature is the prevalent use of the Compact

Tension (CT) specimen [15, 21, 11, 20]. This specimen geometry has a large thickness relative to its width, resulting in a more plane-strain crack tip state. In relation to aerospace applications, many components are made of thin walled structures that exhibit more of a plane-stress state. Generally, it is known that a plane stress state increases the crack growth resistance compared to the triaxial stress state generated in a plane-strain condition [22]. Thus, improvements in crack growth behaviour may be realized in thin-walled applications of SLM Ti-6Al-4V.

Given the importance of understanding crack growth behaviour for applications in safety-critical aerospace components, it is necessary to gain greater confidence in which factors have a strong influence on the crack growth resistance of SLM Ti-6Al-4V. To the authors' best knowledge, no work has been published to date which investigates the impact of any build orientations that are off-axis to one of the three (transverse, parallel or perpendicular) orthogonal orientations. Additionally, no studies have been found that investigate crack growth behaviour on thin specimens that are more representative of a plane-stress condition. This paper aims at investigating these two points, with a focus on improving the understanding of the effects of the build orientation (and resulting columnar grain orientation) on fatigue crack growth properties.

## 2. Methods

Based on the potential influence of material anisotropy on the design of fatigue critical SLM parts, the influence of specimen build orientation within the XZ-plane, where Z is the build direction, on the fatigue crack growth resistance of SLM Ti-6Al-4V was experimentally investigated. The primary goals were to isolate the influence of directionality of elongated columnar grains related to build orientation on the fatigue crack growth rate and crack path behaviours. Five build orientations ( $0^\circ$ ,  $30^\circ$ ,  $45^\circ$ ,  $60^\circ$ , and  $90^\circ$ ) and two post heat treatment conditions were investigated. The second goal was to test specimens with smaller thicknesses that are more representative of thin-walled structures. Details of the testing and measurement methods used in this study are provided in the remainder of this section.

### *2.1. Specimen configuration and fabrication*

The specimen configuration chosen for this study is the Single Edge Notch Tension (SENT). This configuration was chosen over the more common Com-

pact Tension (CT) specimen used in previous studies on crack growth in AM materials [11, 20], mainly due to its improved suitability for specimens with smaller thicknesses. The SENT specimen also enables data collection over a wider range of crack length-to-width ratios ( $a/W$ ) compared to Double Edge Cracked Tension (DENT) and Centre Crack Tension (CCT) specimens, maximizing the data that could be collected for a fixed specimen width. The overall dimensions of the specimen, including starting notch geometry and clamped region of the specimen, are illustrated in Fig. 1.

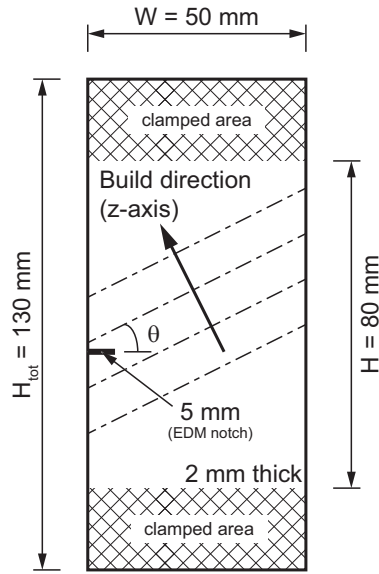


Figure 1: SENT specimen dimensions.

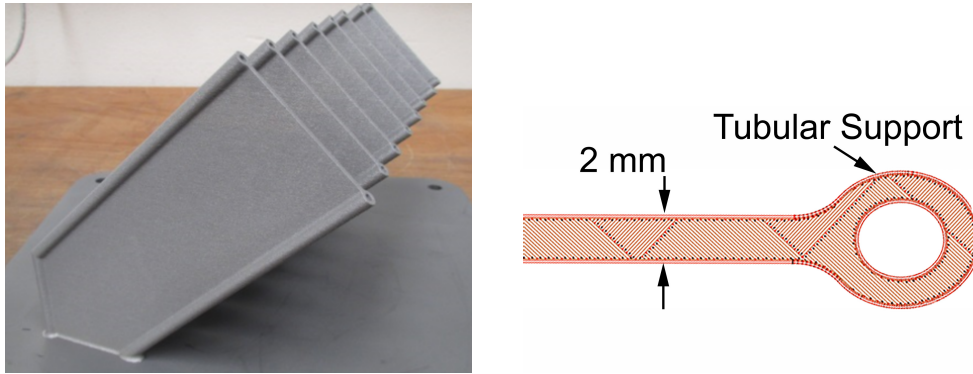
Three factors were taken into consideration when determining the overall size of the SENT specimen. First, the overall length of the specimen was limited by the build volume and available build time of the AM machine. Second, specimen warping due to thermal gradients posed a challenge for manufacturing a thin flat plate. Third, the ASTM standard [23] for the SENT specimen recommends a minimum height-to-width ratio ( $H/W$ ) of 2 in order to avoid the clamped specimen boundary conditions from influencing the standard stress intensity factor solutions for the SENT specimen configuration. Consideration for each of these factors led to the dimensions provided in Fig. 1, although it should be noted that a final  $H/W$  ratio of only 1.6 was realized. This will be further discussed in Section 2.3.

Specimen fabrication was carried out using a SLM Solutions SLM 280 HL machine and Ti-6Al-4V Grade 5 powder with a particle diameter range of 20-63  $\mu\text{m}$ . Specimens were fabricated using a 50  $\mu\text{m}$  layer thickness by first tracing the outer layer contour lines, second performing a second inner contour trace referred to as a contour fill, and finally performing a checkerboard patterned hatch fill. The position and orientation of the hatch fill pattern is altered in each successive layer. Details of the laser scanning power, speed, and intensity for the different laser scanning steps are summarized in Table 1. A tubular support feature (see Fig. 2) was included along both edges of the test specimens during manufacturing in order to increase the out-of-plane specimen stiffness and minimize thermal distortions. The specimens were manufactured in five batches, with each batch comprised of all the specimens for a single build orientation. A stress relief heat treatment was performed on each batch of specimens prior to removal from the build platform by means of electrical discharge machining (EDM). Subsequent to removal, half of the batch received a further HIP treatment. The details of the two overall heat treatments are provided in Table 2 and a sample temperature and pressure history for a HIPed specimen is given in Fig. 3. No specimens were tested in the As-Built condition as the intent of this study was to exclude, as much as possible, influences of residual stresses on crack growth behaviour. Although no residual stress measurements were performed within this study, the work of Knowles [12] confirms the expectations that the heat treatments used within this study should be sufficient for eliminating the majority of residual stresses built-up during manufacturing.

Table 1: Laser scanning process parameters

	Contour Lines	Fill contour	Hatch	Supports
Laser power [W]	100	150	275	150
Scan velocity [mm/s]	400	450	975	750
Laser intensity [W.mm/s]	0.25	0.33	0.28	0.2
Laser spot diameter [ $\mu\text{m}$ ]	50	50	50	50
Line Spacing [mm]	0.084	0.084	0.084	

After the final heat treatment step, the tubular supports were removed by EDM, and the edges of the specimen were milled to reach their final nominal dimensions shown in Fig. 1. This milling step also resulted in a smooth specimen edge, limiting the risk of fatigue cracks nucleating at locations other than the defined notch. The final 5 mm notch was produced via EDM.



(a) batch of 45° specimens on build plate (b) details of scanning strategy and tubular supports

Figure 2: SENT specimen manufacturing details.

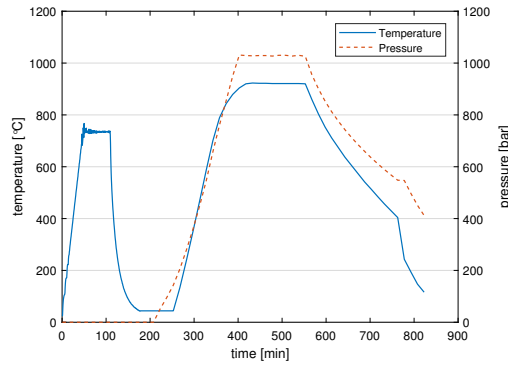


Figure 3: Typical temperature and pressure profile for a HIP specimen.

Table 2: Heat treatment details

Stress Relief treatment (SR)	Hot Isostatic Pressing treatment (HIP)
1. Anneal at $735 \pm 13$ °C for 1 hour	1. Anneal at $735 \pm 13$ °C for 1 hour
2. Furnace cooled under protective Argon atmosphere to room temperature	2. Furnace cooled under protective Argon atmosphere to room temperature
	3. Increase temperature to $920 \pm 13$ °C and pressure to $1000 + 50 / - 0$ bar and hold for 2 hours
	4. Air cool to room temperature

Although measurement of material porosity and static strength were not within the scope of this study, previous studies within the Netherlands Aerospace Centre (NLR) [24] using the same machine and processing parameters provide an indication of the expected material behaviour. In this study, the average porosity after the SR treatment was measured using Archimedes method to be 0.50% and also evaluated from cross sections through the specimen to be 0.17%. For the HIPed condition, porosity was only evaluated from cross sections through the specimens, where for the sections made, no evidence of porosity was observed. Although measuring porosity by means of sectioning only provides a local indication of porosity, and is thus a less reliable measure of overall porosity, this result still provides a strong indication for a reduction in porosity as a result of HIPing. Overall, these results indicate that both the SR and HIPed specimens in this study should not have excessive amounts of porosity. In addition to porosity, the NLR study also investigated the anisotropy in static strength of the material. This study found that the ultimate tensile strength can vary by approximately 10% between the orthogonal build orientations.

In total, five batches of eight specimens were produced. A breakdown of the specimens is provided in Table 3

Table 3: Test matrix

Build Orientation	Stress Relieved	HIP
0°	4 <sup>a</sup>	4 <sup>a</sup>
30°	4	4
45°	4	4
60°	4	4
90°	4	4 <sup>b</sup>

<sup>a</sup>One specimen tested in stepwise loading manner to determine appropriate fatigue loading. Results of this specimen are excluded from results

<sup>b</sup>One specimen, due to excessive curvature, exhibited signs of crack closure on the fracture surface. Results of this specimen are excluded from the results

## 2.2. Fatigue test setup

Fatigue crack growth tests were performed within the Delft Aerospace Structures and Materials Lab (DASML) using a 100 kN MTS servo hydraulic

test frame equipped with MTS 647 hydraulic wedge grips. This frame contained a class-1 100 kN load cell with a calibrated accuracy of 0.2%. A photo of the test setup is provided in Fig. 4.

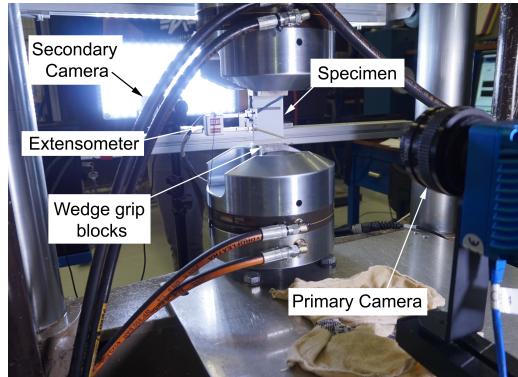


Figure 4: Fatigue test setup.

For specimen placement, the fact that the specimen width equaled the width of the wedge grip blocks was exploited. The notch edge of the specimen was aligned with the end of the wedge grip blocks using a machined alignment block, thereby ensuring the specimen was aligned with the loading axis of the test frame. Vertical placement of the specimen within the grips was confirmed with reference marks drawn on the specimen surface prior to installation.

Fatigue tests were performed under constant amplitude loading. In order to determine the most appropriate fatigue load to use in the study, two specimens were tested in a stepwise increasing fashion, where the fatigue load was increased by 10% every 50,000 cycles. These two specimens are highlighted in the Table 3 by footnote *a*, and have been excluded from the results of the study. Based on the results of these stepwise increasing fatigue tests, a final maximum applied load of 10 kN (corresponding to a nominal applied stress of 100 MPa) with a stress-ratio of 0.1 and test frequency of 10 Hz was selected for the study. All tests were run until complete fracture of the specimen occurred.

### 2.3. Crack growth measurement techniques

Two means of measuring crack growth rate were used in this study. The primary means was through visual measurement of the crack length throughout the duration of the test and subsequent processing of the crack length data using the incremental polynomial method outlined in ASTM E647-00

[23]. A secondary means of measuring crack growth rate was through striation spacing measurement on the fracture surface. Striation spacing measurement is a more direct means of measuring crack growth rate, however, it is more time consuming, thus it was only employed as a means of verification of the crack growth rates obtained through visual crack growth measurements. A third means of measuring crack growth was attempted by measuring the crack opening displacement using an extensometer (visible in Fig. 4) and relating it to the crack length using Linear Elastic Fracture Mechanics (LEFM). However, due to an issue with a connector between the extensometer and the MTS controller, the data obtained contained significant amounts of noise and signal loss. As a result, this means of measuring crack growth is excluded from this paper.

For the visual measurements of the crack growth, a 4 MP camera was used to take an image of the specimen every 1000 cycles. This was achieved by pausing the fatigue test and taking a photo at the maximum applied fatigue load to ensure the best visibility of the open fatigue crack. The crack length could subsequently be measured visually from the image in terms of pixels. A conversion from pixels to mm was obtained for each image from a piece of graph paper with 1 mm spaced lines that was adhered to the specimen and present in the field of view of the camera. Measuring the number of pixels spanning 1 cm of the graph paper in each image, an average conversion factor of 0.03 pixels/cm was obtained. It is estimated that the precision of locating the crack tip was typically  $\pm 5$  pixels, however, lower precision in identifying the crack tip is possible for very short cracks where crack opening is less visible. As a result, crack lengths were recorded to a tenth of a millimeter and a threshold of 0.5 mm was placed on subsequent crack length measurements. The obtained crack length vs. cycles data was subsequently processed into crack growth rate using the 7-point incremental polynomial method outlined in ASTM E647-00 [23].

For determining the crack growth rate from striation spacings, the fracture surface of the tested specimens was observed in a JOEL JSM 7500F field emission scanning electron microscope (SEM). Conveniently, the entire width of the fracture surface could fit within the SEM chamber, allowing the whole specimen to be viewed and the coordinates of points on the fracture surface to be determined by specifying the root of the EDM notch as the datum and measuring position using the traveling stage of the SEM. Crack growth rates were calculated by determining the average growth rate for a spacing measured across 5 striations.

Crack growth rate is typically plotted against the cyclic stress intensity factor range,  $\Delta K$ . Classical LEFM solutions exist for specific crack geometries, including the SENT specimen configuration. These solutions are typically expressed using non-dimensional geometric correction factors ( $\beta$ -factors) that modify the  $K$ -solution for a crack in an infinite sheet using:

$$\Delta K = \beta \Delta \sigma \sqrt{\pi a} = (\beta_{\text{Tada}}) (\beta_{\text{FEM}}) \Delta \sigma \sqrt{\pi a} \quad (1)$$

where  $\beta$  is the non-dimensional geometric correction factor,  $a$  is the crack length, and  $\Delta \sigma$  is the cyclic far-field stress. For the SENT specimen geometry, Tada [25] provides the  $\beta$ -factor solution as:

$$\beta_{\text{Tada}} = 1.12 - 0.231 \left(\frac{a}{W}\right) + 10.55 \left(\frac{a}{W}\right)^2 - 21.72 \left(\frac{a}{W}\right)^3 + 30.39 \left(\frac{a}{W}\right)^4 \quad (2)$$

where  $W$  is the half-width of the specimen. This solution is only valid for a specimen with a height-to-width ratio ( $H/W$ ) greater than or equal to 2. As mentioned in Section 2.1, the specimen used in this study has an  $H/W = 1.6$  which is smaller than the applicable range for the Tada solution. Thus, an additional  $\beta$  correction factor was used in this study to account for the smaller  $H/W$  ratio:

$$\beta_{\text{FEM}} = 1.0056 - 0.5729 \left(\frac{a}{W}\right) - 0.8072 \left(\frac{a}{W}\right)^2 + 1.5448 \left(\frac{a}{W}\right)^3 - 0.2173 \left(\frac{a}{W}\right)^4 \quad (3)$$

This additional solution is based on Finite Element modeling of the SENT specimen geometry used in this study. Further details on how it was obtained can be found in [26].

In addition to the crack growth rate, the direction of the crack path in terms of deviation from the horizontal EDM notch plane was also measured. This was achieved using similar techniques used in obtaining the visual crack growth measurements. The final fractured specimen was placed on top of a piece of graph paper with 1 mm spaced lines and photographed from above. The coordinates of points along the crack path could then be determined by specifying a datum at the EDM notch aligned with the specimen edge and EDM notch plane.

#### 2.4. Microstructure analysis

The microstructure of fractured specimens was observed using standard metallurgical mounting, polishing, and optical microscopy techniques. The microstructure was observed only on the face of each specimen (within the XZ-plane). Small sections of each specimen were mounted in epoxy pucks for polishing, polished, and subsequently etched for 10 seconds using a solution of 62 wt.% distilled  $H_2O$ , 32 wt.%  $HNO_3$ , and 6 wt.%  $HF$ .

One of the 45° specimens was polished again to obtain a flat surface that is suitable for electron back scatter diffraction (EBSD) analysis of the texture. The EBSD maps are collected using a FEI NovaNanoSEM 450 with Trident EBSD system from EDAX. Two scans were made; one overview scan of an area of 412 x 412  $\mu m$  using a step size of 0.55  $\mu m$  and one detail scan of an area of 165 x 165  $\mu m$  using a step size of 0.25  $\mu m$ . The obtained data was analysed using the OIM software from EDAX that belongs to the EBSD system. The data was cleaned using the grain CL standardization CIS filter and neighbour orientation correction NCIC filter with L=1. The data is rotated over 90 over TD to obtain the orientation perpendicular to the fracture plane. Only the data of the alpha-titanium is shown in the figures.

### 3. Results

#### 3.1. Microstructure

At low magnification, all specimens exhibited a columnar grain structure commonly observed within the XZ plane of SLM Ti-6Al-4V [13, 10, 27]. This grain structure is associated with the epitaxial growth of prior  $\beta$  grains during the SLM process. The orientation of these grains was observed to deviate between 5°-15° from the build direction (see Fig. 5). Such deviations in growth direction are a result of directional cooling of the local melt pool [11] and are dependent on the scanning speed and strategy used in the AM process [10].

At higher magnification, the columnar prior  $\beta$  grains were found to be filled with a mixture of fine needle  $\alpha$  phase distributed within a  $\beta$  phase (see Fig. 6). The SLM process is known to result in a complete martensitic  $\alpha'$  microstructure in the As-Built condition [27, 13, 10]. During the stress relieving and/or HIP treatments used in this study the temperature is raised, but kept below the  $\beta$  transus, resulting in a transformation of the martensitic structure into an  $\alpha + \beta$  mixture. The higher temperature of the HIP treatment results in a coarser  $\alpha$  plate structure compared to specimens receiving

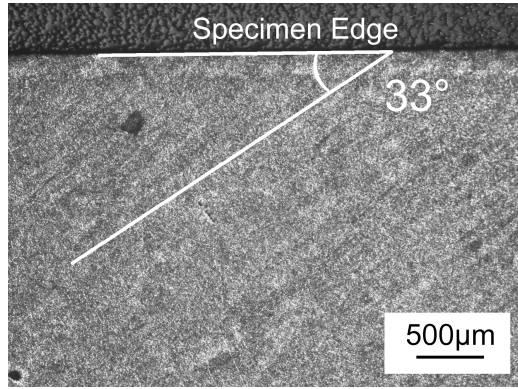
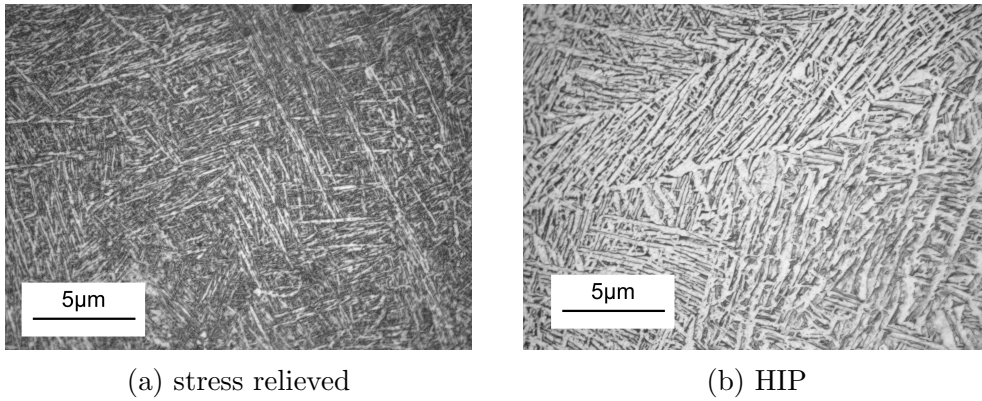


Figure 5: Columnar grain alignment relative to specimen edge for  $45^\circ$  build orientation as seen on the specimen surface.



(a) stress relieved

(b) HIP

Figure 6: Typical observed micro-structure for stress relieved and HIP states.

only the stress relieving treatment, as observed in Fig. 6. These base microstructural observations are consistent with previous studies on the effect of the SLM process and subsequent heat treatments on the microstructure of SLM Ti-6Al-4V [27, 13, 10].

With respect to the different build orientations, no distinct differences were observed in the microstructure within the macroscopically visible columnar grains. This observation is further supported by the EBSD texture measurements which did not show any dominant grain orientation within the macroscopic columnar grains.

The two EBSD scans give the same general texture information. The image of the detail scan is shown in Fig. 7. The overview image is not

shown because the image quality is poorer due to the larger step size and the information in the image is the same as in the detail image. The pole figures are shown in Fig. 8 for both the detail image and the overview image.

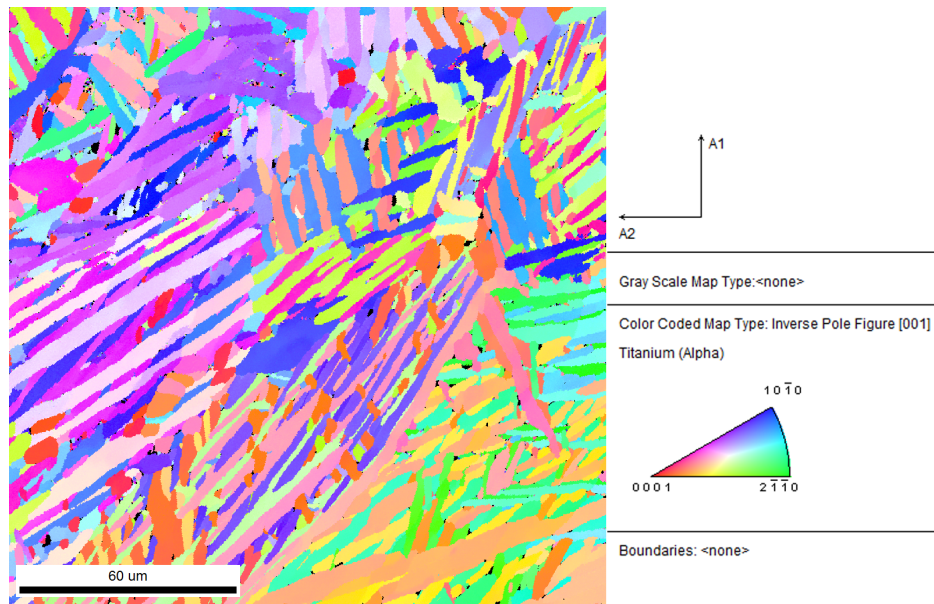


Figure 7: EBSD map showing the  $\alpha$  plates with their orientation.

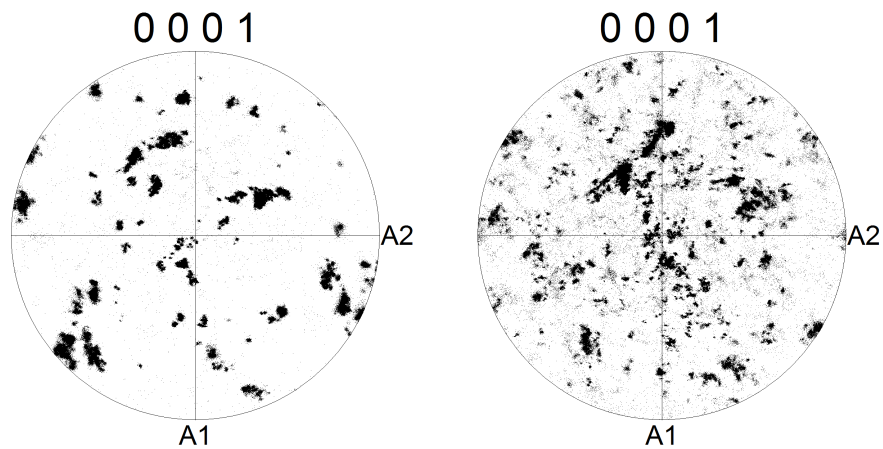


Figure 8: Pole figures for detail scan (left) and overview scan (right), showing no preferred orientation.

No preferred orientation can be observed. The grain size is of the order of  $50\ \mu\text{m}$  in width, which implies that more than 10 grains will be present in the thickness of the specimens. These two observations mean that the crack tip encounters multiple grains with different orientations at the same time.

### 3.2. Crack path

The columnar grain structure of the specimens fabricated in this study have the potential of introducing anisotropy in material properties that could create preferential fracture planes. Previous studies in the literature have reported differences in static fracture properties of SLM Ti6Al4V for the three orthogonal orientations with respect to the build platform, suggesting the existence of preferential fracture planes [27, 13, 20, 28]. Such preferential planes could influence the path of the fatigue crack for the various build orientations tested in this study.

The fracture paths for the different build orientations tested are provided in Fig. 9. The raw data for the plots has been made available online [29]. The axes in Fig. 9 have a 1:1 scaling ratio such that the observed crack path deviation is not exaggerated and to allow the crack path slope to be easily compared to the build orientation angle. Generally speaking, the observed crack path deviation from the original EDM notch plane is quite small. Greater deviations are observed for the  $30^\circ$  and  $45^\circ$  build orientations, however the majority of this deviations occurs in the last 20% of the specimen width where unstable crack growth occurs (largest recorded crack length in any test prior to static failure was 39.6 mm). No clear differences in overall trend were observed between the HIPed and stress relieved specimens.

Sections of fractured specimens were mounted and polished to observe any potential interactions between the crack path and the local microstructure. A representative result is provided in Fig. 10 showing that in local regions the crack path does indeed orient itself with respect to the fine needle  $\alpha$  plates in the material. However, in an equal number of areas, the crack path passes transversely through these  $\alpha$  plates. Overall, no distinct difference was observed between the interaction of the fracture path and the local microstructure that would indicate a significant role of the columnar grain orientation on the fracture behaviour. Furthermore, due to the length scale of these changes between fracture following and traversing the  $\alpha$  plates be much smaller than the crack length measurement accuracy, it was not possible to observe a potential influence on crack growth behaviour.

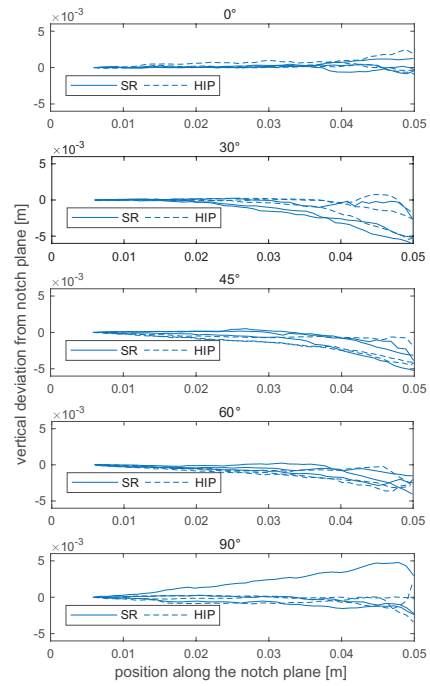


Figure 9: Observed deviations in crack path from the notch plane.

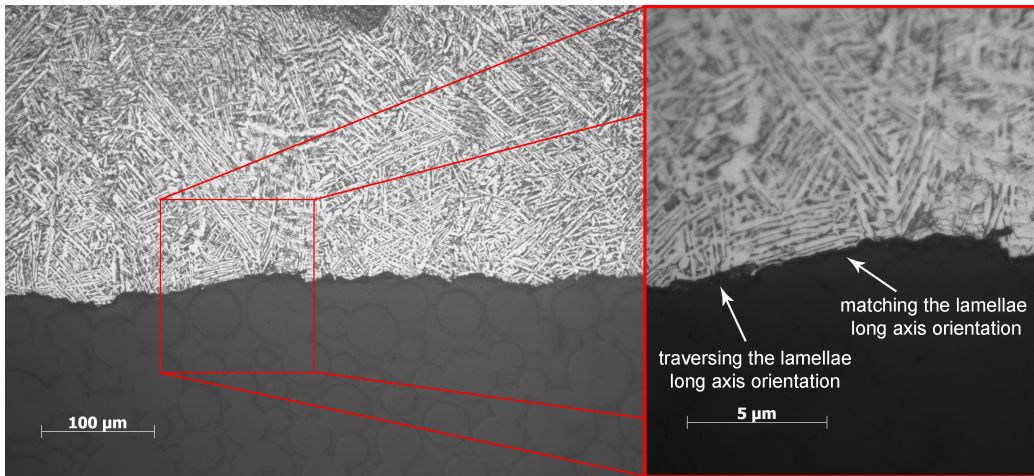


Figure 10: Alignment of the fracture plane with local microstructure for 0° HIP specimen.

### 3.3. Crack growth curves

Although the orientation of columnar grains was not observed to have a significant influence on crack path (ie: crack planes did not preferentially

follow the columnar grain boundaries), it could potentially influence fatigue crack growth resistance.

The primary method for determining the crack growth curves in this study was through visual measurement of the crack length using a digital camera and processing these crack lengths using the incremental polynomial method detailed in ASTM E647-00[23]. The overall crack growth curves obtained via this procedure are given in Fig. 11, including log-linear fits of the data and lines indicating the 95% confidence intervals of these fits. The fitting parameters are provided in Table 4. When reviewing these figures, the reader is reminded that the data for the 90° orientation is comprised of one less specimen than the other orientations, which may produce a false sense of reduced scatter for this orientation. The raw crack length vs. cycles data and the scripts used to calculate the crack growth rates have been made available online [29].

Table 4: Log-linear fitting parameters for Paris Relation (95% confidence interval values in brackets).

Build Orientation	C	m
0° SR	$6.74 \times 10^{-10}$ ( $4.56 \times 10^{-10}$ , $9.86 \times 10^{-10}$ )	1.85 (1.74, 1.96)
0° HIP	$6.28 \times 10^{-10}$ ( $4.34 \times 10^{-10}$ , $9.19 \times 10^{-10}$ )	1.87 (1.76, 1.98)
30° SR	$2.73 \times 10^{-9}$ ( $1.97 \times 10^{-9}$ , $3.80 \times 10^{-9}$ )	1.47 (1.37, 1.56)
30° HIP	$3.47 \times 10^{-9}$ ( $2.13 \times 10^{-9}$ , $5.67 \times 10^{-9}$ )	1.44 (1.30, 1.58)
45° SR	$3.18 \times 10^{-9}$ ( $2.47 \times 10^{-9}$ , $4.04 \times 10^{-9}$ )	1.45 (1.38, 1.52)
45° HIP	$4.88 \times 10^{-9}$ ( $3.21 \times 10^{-9}$ , $7.43 \times 10^{-9}$ )	1.33 (1.21, 1.45)
60° SR	$2.31 \times 10^{-9}$ ( $1.56 \times 10^{-9}$ , $3.44 \times 10^{-9}$ )	1.56 (1.44, 1.67)
60° HIP	$3.51 \times 10^{-9}$ ( $2.40 \times 10^{-9}$ , $5.18 \times 10^{-9}$ )	1.42 (1.30, 1.57)
90° SR	$9.66 \times 10^{-10}$ ( $5.69 \times 10^{-10}$ , $1.64 \times 10^{-9}$ )	1.80 (1.64, 1.95)
90° HIP	$2.17 \times 10^{-9}$ ( $1.40 \times 10^{-9}$ , $3.37 \times 10^{-9}$ )	1.45 (1.33, 1.58)

The axes in Fig. 11 have been scaled to maximize the visibility of the data and its variation within this study. Scatter in behaviour is observed between specimens of the same build orientation and for both heat treatments. When looking at the degree of scatter for individual orientations compared to all orientations, it is not possible to discern conclusively any differences in crack growth behaviour. For the same reason, it is not possible to discern clear differences between the stress relieved and HIPed heat treatment conditions.

Given the procedure for calculating crack growth rate and its potential sensitivity to the frequency and accuracy of crack length measurements, a

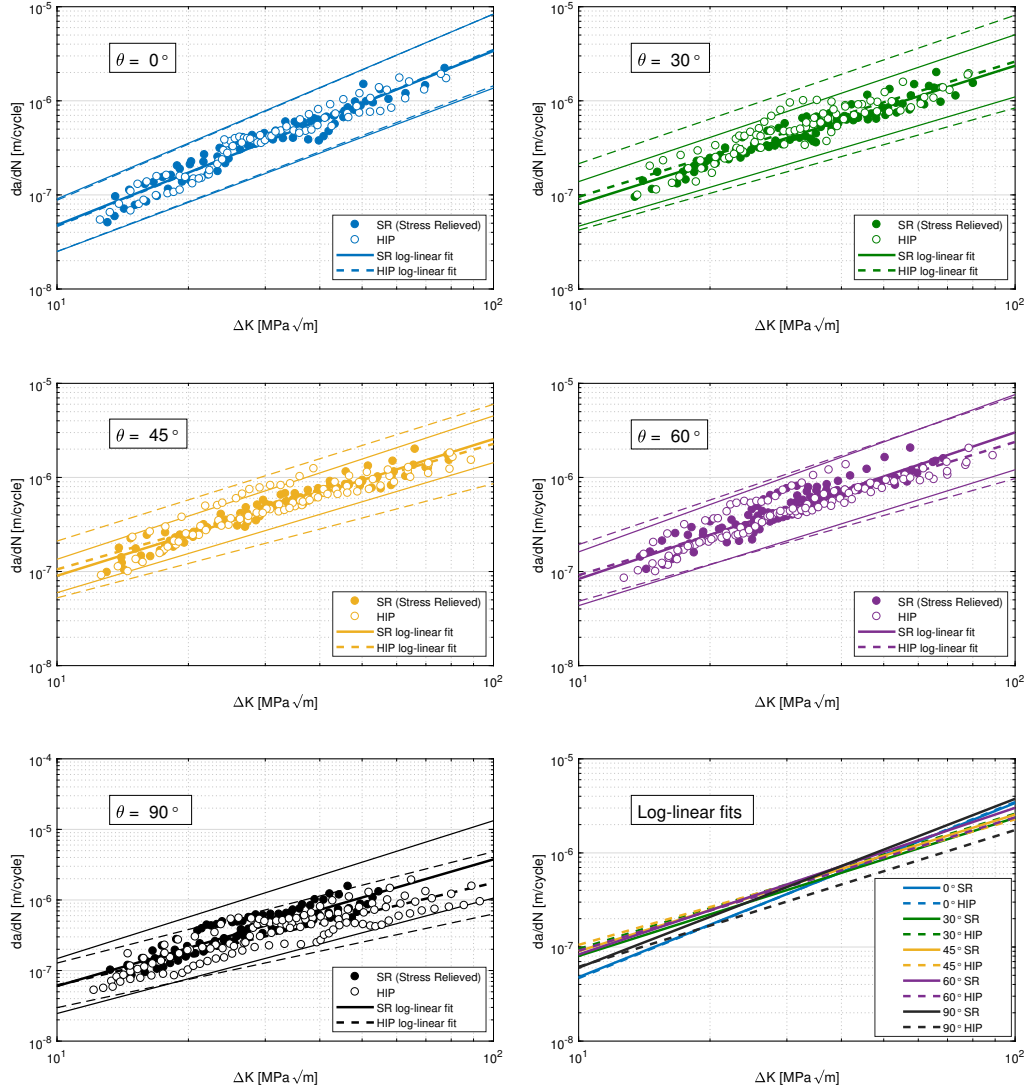


Figure 11: Comparison of calculated fatigue crack growth rates for different build orientations. Thin lines indicate 95% confidence intervals of log-linear fits.

second measurement approach was used to increase confidence in the measurements. These measurements were performed by measuring the striation spacing on the fracture surface of one of the fatigue specimens using a SEM. All measurements were as an average across five striations as shown in Fig.

12. A sample of these measurements for a stress relieved 60° build direction specimen are shown in Fig. 13. The good agreement between the incremental polynomial calculations and the SEM measurements increases the confidence in the overall data set shown in Fig. 11 and that the observed scatter is not likely due to measurement inaccuracies.

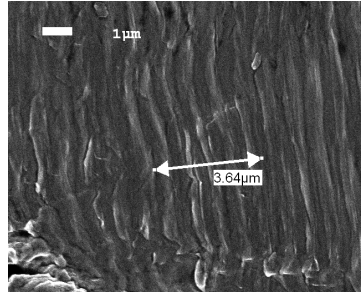


Figure 12: Sample SEM image showing 5-striation spacing measurement.

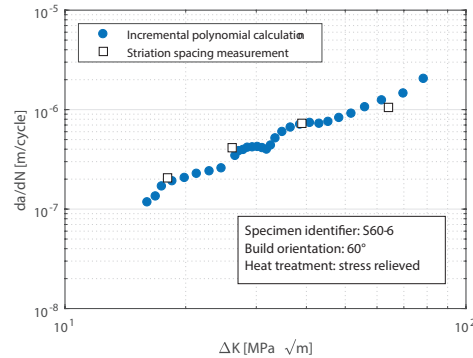
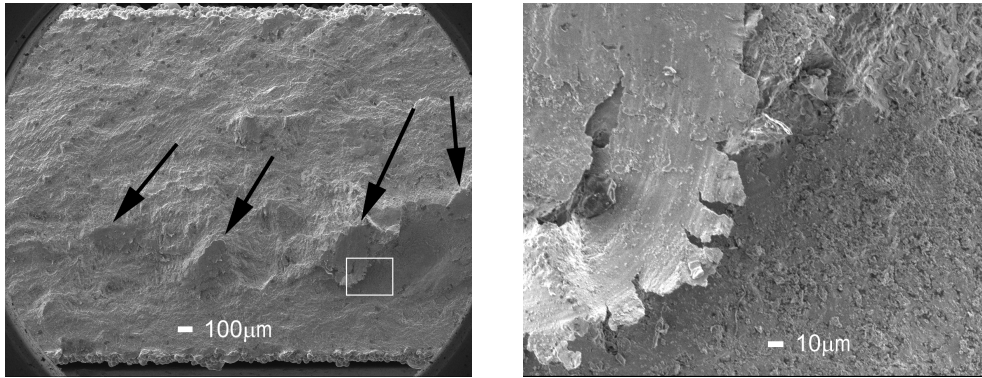


Figure 13: Comparison of crack growth rates determined by incremental polynomial calculation and SEM striation spacing.

Lastly, footnote b in Table 3 requires some additional scrutiny in order for the reader to be satisfied with the decision to exclude the data from this study. Indeed, the crack growth data for this single specimen was found to exhibit a significantly lower crack growth rate behaviour than all other tested specimens. However, on close examination of the fracture surface, it was found that there were numerous matching scars on both sides of the fracture surface that indicated significant contact between the crack flanks during testing. An example of these scars is shown in Fig. 14 highlighted



(a) arrows indicating fracture surface scars      (b) detail view of a single scar

Figure 14: Example of scars observed on the fracture surface of the excluded test specimen.

by the black arrows. It is hypothesized that these scars are a result of crack flank contact during testing initiated by curvature in the specimen. All specimens tested showed some degree of curvature resulting from thermal expansion during the build process. Unfortunately, the precise curvature of each specimen was not measured prior to testing. However, the fact that the scars on the fracture surface exhibited a bias towards one face of the specimen is consistent with the hypothesis. Based upon this hypothesis and the fact that these fracture surface scars were only observed on this single specimen, it was decided to remove the specimen from this study as the influence of crack closure on the measured growth rates could not be adequately quantified.

#### 4. Discussion

This investigation was initiated based on a curiosity regarding the potential influence of columnar grain orientation on the crack growth resistance in directions off-axis to the build direction and its implications for a damage tolerance design approach. It was hypothesised that the columnar grain structure could influence either the crack growth resistance and/or crack path, particularly when oriented at an angle other than  $0^\circ$  or  $90^\circ$ . The results from this study, however, indicate that any potential influence from the columnar grain orientation is small and indistinguishable from experimental scatter in the fatigue crack growth measurements. This may be explained with the random orientation of the grains in combination with the much

smaller width of the columns compared to the specimen thickness. A result of these microstructural characteristics of the specimens is that the crack front always encounters multiple grains with different orientations and therefore will not be able to follow the orientation of a particular grain. From an engineering perspective, this result is desirable as it removes the need to strongly consider the build orientation of a specific component in relation to its damage tolerance behaviour. This is ideal as selection of an orientation is highly driven by geometric tolerances, minimum overhangs, and other production-driven considerations. It should be noted that the overall fatigue behaviour of a part may not be entirely independent of orientation, as the surface finish/quality of a part and the geometric tolerances of highly stressed regions are both dependent on orientation with respect to the build direction. Results from this study only indicate that the crack growth behaviour is not strongly influenced by build orientation.

With respect to damage tolerance, it is also important to reflect on the influence of the heat treatment on the fatigue properties. Porosity within the material can exacerbate the initiation of fatigue cracks in part due to the local stress concentration they provide within a material. HIPing is a process which is meant to reduce the amount and size of such pores, which was confirmed for the processing parameters used in this study in a previous NLR study [24]. Even though the porosity level in non-HIPed specimens can be quite low (0.50% as observed in [24]), this reduction can still have a significant impact on the overall fatigue life as confirmed by Leuders et al. [11]. The damage tolerance philosophy is intended to address the potential risk of defects, such as low levels of porosity, by assuming they are present and form fatigue cracks at the very beginning of the component's life. Based on the crack growth life of the component, regular inspection intervals can be defined to ensure that any fatigue damages that could occur can be detected and repaired before they become critical to structural integrity. Thus, the crack growth behaviour is of primary concern for a damage tolerance analysis. From the results of this study, it is clear that the reduction in porosity due to HIPing does not have a significant influence on crack growth behaviour. This can be explained by the fact that the base amount of porosity in the SR specimens is expected to be already very low (around 0.50%) which is not expected to have a significant effect on crack growth. Indeed, very high levels of porosity could be expected to have an influence on crack growth behaviour, but such materials would likely be deemed of too poor quality for application in the aerospace industry and are thus not considered in this

discussion. This lack of influence on crack growth behaviour suggests that for high quality SLM materials (ie: with already low porosity and other internal defects), a HIPing process can reduce the risks of early crack initiation but will not greatly affect inspection intervals resulting from a damage tolerance analysis to mitigate these risks. This is important to consider in terms of the life-cycle costs of AM parts in the aerospace industry.

Within the literature, some studies have indicated an influence of build orientation on crack growth behaviour, particularly in the AB condition [11], while other studies indicate that no variation was observed [15, 21]. Furthermore, those same studies indicated that the greatest difference in crack growth behaviour was observed between AB specimens and specimens subjected to some form of annealing heat treatment known to relieve some of the residual stresses. These results suggest that residual stresses play a substantial role on observed variations in crack growth behaviour. Although the residual stress state was not measured for the specimens tested in this study, the heat treatments used are expected to be effective in significantly reducing residual stresses based on other studies within the literature [11, 12]. The results of this study thus support the conclusion that residual stresses play a more dominant role in variations in crack growth behaviour compared to build orientation and heat treatment.

It should be noted that the above discussions are based on comparisons of experimental results where heat treatments and specimen orientation within a build chamber are the primary variables of study. The authors acknowledge that there will likely be a significant influence on processing parameters related to laser and scanning processing parameters within the SLM process, however as such parameters were fixed in this study, and not all studies referenced within the literature here include a complete documentation of processing parameters, it is not possible to critically discuss the precise influence of all of these processing parameters within this study. Indeed, processing parameters are often protected and treated as intellectual property by various AM part producers and research groups, making such an investigation based on published literature difficult. The authors recommend that a greater transparency in processing parameters be sought by the research community in order to facilitate a greater understanding in the AM process and its influence on material and structural properties.

A secondary goal of this study was to examine the fatigue crack growth behaviour in a state closer to plane stress than previous studies utilizing the relatively thick CT-specimen [20, 11]. For this comparison, the overall

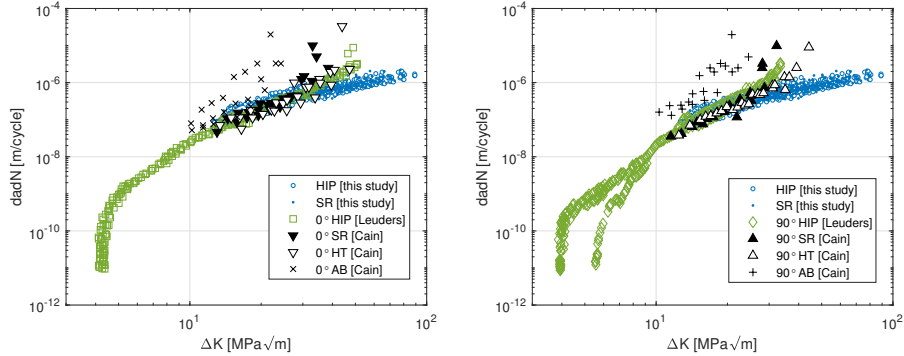


Figure 15: Comparison of crack growth results to studies by Cain [20] and Leuders [11].

results of this study are replotted in Fig. 15 against the data from Leuders and Cain. The data from Leuders and Cain was obtained from images of the relevant plots from their publications using the open source Engauge Digitizer Software [30]. For the data from Cain [20], the software was able to isolate individual data points accurately; however, the data from Leuders [11] contained too many overlapping data points, requiring the user to manually select points to construct the data set. Thus, this data set is not precisely reproduced, but provides an adequate reproduction of the data set for comparison purposes.

From the comparison of the results in Fig. 15, a few observations can be made. First, the degree of scatter in the results from this study between the SR and HIPed specimens, and between repeated tests of the same condition are comparable with that observed in previous studies. Second, the data sets from Cain and Leuders exhibit the beginnings of the asymptotic region of the  $da/dN$  vs.  $\Delta K$  curve associated with static fracture between  $\Delta K$  values of 40 to 50  $\text{MPa}\sqrt{\text{m}}$ , while the data from the present study reaches higher  $\Delta K$  values approaching 80 to 90  $\text{MPa}\sqrt{\text{m}}$ . This is expected as the fracture toughness in a state of plane stress is higher than that of a state of plane strain due to the lower degree of crack tip constraint [22]. Overall, the crack growth behaviour is generally consistent with these other studies, indicating a high degree of consistency in the crack growth behaviour of SLM Ti-6Al-4V produced using different machines and potentially differing processing parameters. This is a promising result in terms of the robustness and consistency of the SLM process and concerns with respect to repeatability in part quality from different machines.

## 5. Conclusions

The aim of this study was to investigate the fatigue crack growth behaviour of SLM Ti-6Al-4V in relation to the specimen build orientation within the XZ-build plane, where the Z-axis refers to the layer normal direction (build direction) in the SLM process. Five orientations with respect to the Z-axis were studied, namely 0°, 30°, 45°, 60°, and 90°. Variations in columnar grain orientation as well as residual stress distribution can be expected by varying the build orientation of the specimen within this plane. To eliminate the latter influence from this study, only specimens that were subjected to post-production heat treatments to limit residual stresses were tested. A standard stress relieving heat treatment and a Hot Isostatic Pressing (HIP) treatment were used for this purpose. The first metric of fatigue crack growth behaviour studied is fatigue crack growth rate. Based on the results of this study, the following key observations were made in relation to this metric:

- Build orientation within the XZ-plane does not have a significant influence on fatigue crack growth rate. Results from one build orientation could not be discerned from the scatter bands of any other build orientation.
- The stress relieving heat treatment and HIP treatment did not have a significant influence on fatigue crack growth rate. Results from one heat treatment could not be discerned from the scatter bands of the other heat treatment.

The second metric of fatigue crack growth behaviour studied is crack path. For this metric, the following key observations were made:

- Build orientation had a small, but repeatable influence on crack path. The influence is likely too small to be of any practical importance.
- The above influence was affected by heat treatment, where HIPed specimens exhibited a smaller influence.

All of the observations above suggest that columnar grain orientation in SLM Ti-6Al-4V does not have a significant influence on fatigue crack growth performance. Furthermore, it suggests that fatigue crack growth behaviour variations observed in the literature, particularly for the as-built condition,

are likely related to variations in residual stress rather than columnar grain orientation.

The results and conclusions of this study should be considered in the context of the AM process, processing parameters, and material type used in the study. Indeed, different materials and AM processing parameters can both result in different material states, each with their own potential for anisotropy.

- [1] ASTM, Standard Terminology for Additive Manufacturing – General Principles Terminology, ASTM International i (2015) 1–9.  
URL [http://compass.astm.org/EDIT/html\\_annot.cgi?ISOASTM52900+15](http://compass.astm.org/EDIT/html_annot.cgi?ISOASTM52900+15)
- [2] PricewaterhouseCoopers LLP, Turning additive manufacturing into business, Tech. rep., PricewaterhouseCoopers LLP, Delaware (2014).
- [3] S. Mellor, L. Hao, D. Zhang, Additive manufacturing: A framework for implementation, *International Journal of Production Economics* 149 (2014) 194–201. doi:10.1016/j.ijpe.2013.07.008.
- [4] V. Petrovic, J. Vicente Haro Gonzalez, O. Jordá Ferrando, J. Delgado Gordillo, J. Ramón Blasco Puchades, L. Portolés Griñan, Additive layered manufacturing: sectors of industrial application shown through case studies, *International Journal of Production Research* 49 (4) (2011) 1061–1079. doi:10.1080/00207540903479786.
- [5] D. Bourell, M. Leu, D. Rosen, Roadmap for Additive Manufacturing: Identifying the Future of Freeform Processing, Tech. rep., The University of Texas at Austin, Austin, TX (2009).
- [6] I. Gibson, D. Rosen, B. Stucker, *Additive Manufacturing Technologies: 3D Printing, Rapid Prototyping, and Direct Digital Manufacturing*, Second Edition, 2nd Edition, Springer, New York, 2015. doi:10.1007/978-1-4939-2113-3.  
URL <http://www.ciri.org.nz/nzrma/technologies.html>
- [7] G. Lütjering, J. Williams, *Titanium*, 2nd Edition, Berlin Heidelberg, 2007. doi:10.1007/978-3-540-73036-1.
- [8] D. D. Gu, W. Meiners, K. Wissenbach, R. Poprawe, Laser additive manufacturing of metallic components: materials, processes and

- mechanisms, *International Materials Reviews* 57 (3) (2012) 133–164. doi:10.1179/1743280411Y.0000000014.
- [9] A. M. Beese, B. E. Carroll, Review of Mechanical Properties of Ti-6Al-4V Made by Laser-Based Additive Manufacturing Using Powder Feedstock, *The Journal of The Minerals, Metals & Materials Society (JOM)* 68 (3) (2016) 724–734. doi:10.1007/s11837-015-1759-z.
- [10] L. Thijs, F. Verhaeghe, T. Craeghs, J. V. Humbeeck, J. P. Kruth, A study of the microstructural evolution during selective laser melting of Ti-6Al-4V, *Acta Materialia* 58 (9) (2010) 3303–3312. doi:10.1016/j.actamat.2010.02.004.  
URL <http://dx.doi.org/10.1016/j.actamat.2010.02.004>
- [11] S. Leuders, M. Thne, A. Riemer, T. Niendorf, T. Trster, H. Richard, H. Maier, On the mechanical behaviour of titanium alloy ti6al4v manufactured by selective laser melting: Fatigue resistance and crack growth performance, *International Journal of Fatigue* 48 (2015) 300–307.
- [12] C. R. Knowles, Residual stress measurement and structural integrity evaluation of slm ti-6al-4v, *South African Journal of Industrial Engineering* 23 (3) (2012) 119–129.
- [13] B. Vrancken, L. Thijs, J.-P. Kruth, J. Van Humbeeck, Heat treatment of ti6al4v produced by selective laser melting: Microstructure and mechanical properties, *Journal of Alloys and Compounds* 541 (2012) 177–185. doi:10.1016/j.jallcom.2012.07.022.
- [14] B. V. Hooreweder, D. Moens, R. Boonen, J.-P. Kruth, P. Sas, Analysis of fracture toughness and crack propagation of ti6al4v produced by selective laser melting, *Advanced Engineering Materials* 14 (1-2) (2012) 92–97.
- [15] N. M. Dhansay, R. Tait, T. Becker, Fatigue and Fracture Toughness of Ti-6Al-4V Titanium Alloy Manufactured by Selective Laser Melting, *Advanced Materials Research* 1019 (2014) 248–253. doi:10.4028/www.scientific.net/AMR.1019.248.
- [16] P. Edwards, M. Ramulu, Fatigue performance evaluation of selective laser melted Ti6Al4V, *Materials Science and Engineering: A* 598 (2014) 327–337. doi:10.1016/j.msea.2014.01.041.

- [17] S. Leuders, T. Lieneke, S. Lammers, T. Trster, T. Neindorf, On the fatigue properties of metals manufactured by selective laser melting the role of ductility, *Journal of Materials Research* 29 (17) (2014) 1911–1919. doi:10.1557/jmr.2014.157.
- [18] C. Qiu, N. Adkins, M. Attallah, Microstructure and tensile properties of selectively laser-melted and of hiped laser-melted ti6al4v, *Materials Science and Engineering: A* 578 (2013) 230–239. doi:10.1016/j.msea.2013.04.099.
- [19] ASTM, ISO/ASTM 52921:2013(E): Standard Terminology for Additive Manufacturing Coordinate Systems and Test Methodologies, ASTM Internationaldoi:10.1520/F2921.  
URL [www.astm.org](http://www.astm.org)
- [20] V. Cain, L. Thijs, J. V. Humbeeck, B. V. Hooreweder, R. K. a, Crack propagation and fracture toughness of ti6al4v alloy produced by selective laser melting, *Additive Manufacturing* 5 (2015) 68–76.
- [21] P. Edwards, M. Ramulu, Effect of build direction on the fracture toughness and fatigue crack growth in selective laser melted Ti-6Al-4V, *Fatigue and Fracture of Engineering Materials and Structures* 38 (10) (2015) 1228–1236. doi:10.1111/ffe.12303.
- [22] J. Schijve, *Fatigue of Structures and Materials*, 2nd Ed., 2nd Edition, Springer, Berlin, 2009.
- [23] ASTM, Standard test method for measurement of fatigue crack growth rates, ASTM E647-00, American Society for Testing and Materials, West Conshohocken, PA (2000).
- [24] M. de Smit, R. Huls, L. 't Hoen-Velterop, E. Sprenkeling, Additive Manufacturing for Space Applications - Final report of NLR activities in the PEP2012 study, Report NLR-CR-2015-116, Netherlands Aerospace Centre (NLR) (2015).
- [25] H. Tada, P. C. Paris, G. R. Irwin, *The Stress Analysis of Cracks Handbook*, 3rd Edition, Wiley, 2000.
- [26] J. Michielssen, Fatigue crack growth in selective laser melted ti-6al-4v, Master's thesis, Delft University of Technology (2017).

- [27] N. V. Rafi, H. K. and Karthik, H. Gong, T. L. Starr, B. E. Stucker, Microstructures and mechanical properties of ti6al4v parts fabricated by selective laser melting and electron beam melting, *Journal of Materials Engineering and Performance* 22 (2013) 3872–3883. doi:10.1007/s11665-013-0658-0.
- [28] W. Xu, E. W. Lui, A. Pateras, M. Quin, M. Brandt, In situ tailoring microstructure in additively manufactured ti-6al-4v for superior mechanical performance, *Acta Materialia* 125 (2017) 390–400. doi:10.1016/j.actamat.2016.12.027.
- [29] C. Rans, J. Michielssen, M. Walker, W. Wang, L. 't Hoen-Velterop, Influence of specimen build orientation on the fatigue crack growth resistance of selective laser melted ti-6al-4v, [Online] (30-Nov-2017). doi:10.17605/OSF.IO/5ATB7.  
URL [osf.io/5atb7](https://osf.io/5atb7)
- [30] M. Mitchell, B. Muftakhidinov, T. Winchen, Z. Jdrzejewski-Szmek, Engauge digitizer software (version 10.0) (2017).  
URL <http://markumitchell.github.io/engauge-digitizer>